Journal of Photochemistry and Photobiology A: Chemistry 230 (2012) 23–30

Contents lists available at SciVerse ScienceDirect

Journal of Photochemistry and Photobiology A: Chemistry

journal homepage: www.elsevier.com/locate/jphotochem

Thermodynamic and conformational investigation of the influence of CdTe QDs size on the toxic interaction with BSA

Qisui Wang[a,b], Pengfei Liu[a], Xiaolan Zhou[c], Xiaolei Zhang[a], Tingting Fang[a], Peng Liu[a,d,*], Xinmin Min[a,b], Xi Li[a,d]

[a] Department of Chemistry, School of Sciences, Wuhan University of Technology, Wuhan 430070, PR China
[b] State Key Laboratory of Advanced Technology for Materials Synthesis and Processing, School of Materials Science and Engineering, Wuhan University of Technology, Wuhan 430070, PR China
[c] Department of Electronic Engineering, Artillery Academy of PLA, Hefei Artillery Academy of PLA, Hefei 230031, PR China
[d] Institute of High Pressure and Temperature Physics, School of Sciences, Wuhan University of Technology, Wuhan 430070, PR China

ARTICLE INFO

Article history:
Received 16 August 2011
Received in revised form
13 December 2011
Accepted 28 December 2011
Available online 5 January 2012

Keywords:
Quantum dot
BSA
Size
Thermodynamic parameter
Conformational change

ABSTRACT

Water-soluble fluorescent colloidal quantum dots (QDs) have been widely used in some biological and biomedical fields, so the interaction of QDs with biomolecules recently attracts increasing attention. In this study, the fluorescence (FL) quenching method, circular dichroism (CD) technique, attenuated total reflection-Fourier transform infrared (ATR-FTIR) and UV–vis absorption spectra were used to investigate systematically the influence of CdTe QDs size on the toxic interaction with bovine serum albumin (BSA). Three size CdTe QDs with maximum emission of 543 nm (green-emitting QDs, GQDs), 579 nm (yellow-emitting QDs, YQDs) and 647 nm (red-emitting QDs, RQDs) were tested. The Stern–Volmer quenching constant (K_{sv}) at different temperatures, corresponding thermodynamic parameters (ΔH, ΔG and ΔS), and information of the structural features of BSA were gained. The FL results indicated that QDs can effectively quench the FL of BSA in a size-dependent manner, electrostatic interactions play a major role in the binding reaction, and the nature of quenching is static, resulting in forming QDs–BSA complexes. The CD and ATR-FTIR spectra showed that the secondary structure of BSA was changed by QDs, indicating the toxic on protein.

1. Introduction

Quantum dots (QDs, semiconductor nanocrystals) are versatile inorganic probes with unique photophysical properties, such as narrow and size-dependent fluorescence (FL) with broad absorption spectra, strong FL intensity, and excellent anti-photobleaching[1–5]. Since Alivisatos and Nie et al. [4,5] demonstrated the application of QDs for biology. QDs have been used in a diverse range of biological applications such as cell labeling, genomic detection, optical sensors, bioimaging[6–9].

Owing to the tremendous focus on applying QDs, there has been increasing interest in an investigation the toxicity of QDs [10–16]. In order to explore the bioeffect of QDs on organisms, there are lots of studies about the interactions between QDs and protein [17–21]. There are at least two potential reasons for study QDs on protein: (i) QDs can be combined with proteins in vivo and thus impact the structure and function of protein [22,23]; (ii) protein was used to modify QDs in many applications, e.g., ion sensors, fluorescence resonance energy transfer, and chemiluminescence resonance energy transfer [24–26]. For example, in order to elucidate the fate of QDs introduced to organism, the interactions between QDs and human serum albumin (HSA) were systematically investigated by various spectroscopic techniques under the physiological conditions. The thermodynamic parameters and the quenching constant were obtained. It was suggested that the binding of QDs and HSA is a result of the formation of QDs–HSA complex and electrostatic interactions play a major role in stabilizing the complex [23]. In another study, Han et al. thought hydrophobic force and sulphydryl group played a key role in the QDs–protein interaction [27]. Furthermore, Zhou's results showed hydrogen bonds and van der Waals interactions played a major role in the binding reaction between QDs and protein [22]. Though the above scholars have already started to research the bioeffect of QDs on protein and got different results, synthetic methods of QDs are various, and each kind of QDs has its own physical and chemical properties, including size, charge, biological activity of their surface coating materials, stability, etc., which determine the toxicity of QDs associate with

* Corresponding author at: Department of Chemistry, School of Sciences, Wuhan University of Technology, Wuhan 430070, PR China. Tel.: +86 27 63410197; fax: +86 27 87863157.
E-mail addresses: wangqisui520@163.com (Q. Wang), chemliup@whut.edu.cn (P. Liu).

1010-6030/$ – see front matter © 2012 Elsevier B.V. All rights reserved.
doi:10.1016/j.jphotochem.2011.12.014

environmental conditions, that is, the interactions between QDs and protein depend on the size, charge, capping agent of QDs and so forth. Xiao et al. thought those differences may be caused by the different QDs sizes [28,29]. However, few reports have focused on the effect of QDs size on the interaction between QDs and protein. As we know, the smaller nanomaterials (QDs) have the more surface energy, so there are the different active when binding with groups of biomolecule (protein). Thus, the results of studies presently are not enough, and it is necessary to continue to study the interaction between different sizes QDs and protein for further investigating the biological effects of QDs.

Here, we choose BSA as our protein model because of its medicinal importance, low cost, ready availability, and unusual ligand-binding properties [22,30]. Three different size CdTe/MPA QDs are selected as the protein receptor. The fluorescence quenching method and CD technique were used to investigate the influence of CdTe QDs size on the toxic interaction with BSA. It was proven that the binding of QDs and BSA is a result of the formation of QDs–BSA complex and electrostatic interactions play a major role in stabilizing the complex. The Stern–Volmer quenching constant (K_{sv}) at different temperatures, corresponding thermodynamic parameters (ΔH, ΔG and ΔS), and information of the structural features of BSA were gained.

2. Material and methods

2.1. Materials

Mercaptopropanoic acid (MPA), cadmium chloride ($CdCl_2$), tellurium (Te), sodium borohydride ($NaBH_4$), ethanol (C_2H_5OH), sodium hydroxide (NaOH), tris (hydroxymethyl) aminomethane, bovine serum albumin (BSA), and other routine chemicals were purchased from Shenshi Chem. Ltd. All the chemicals used were of analytical grade and double distilled deionized water was used in all experiments.

2.2. Instrumental

All FL measurements were recorded using a RF-5301 (Shimadzu) and F-4500 (Hitachi) fluorometers. A Lambda 35 (PerkinElmer) Spectrophotometer was used with a cell of 1.0 cm path length. The CD spectra were recorded on Jasco (J-810-150S) automatic recording spectropolarimeter, using a cylindrical cuvette with 0.1 cm path length. The CD profiles were obtained by employing a scan speed of 100 nm/min and response time of 0.5 s.

3. Methods

A 2 mL solution, containing appropriate concentration of QDs was added to 10 μM BSA solution and mixed. UV–visible spectra of all solutions were recorded in the range of 200–800 nm.

A known concentration of QDs in Tris–HCl buffer solution was added to 10 μM BSA solution and mixed at 298, 304, and 310 K. The fluorescent intensity of the solution was recorded at excitation wavelength of 280 nm using an F-4500 fluorometer, with slit widths for excitation and emission at 5 nm.

For the CD experiment, the concentration of BSA was kept at 10 μM. Far-CD spectra were recorded from 200 to 260 nm in 0.05 M Tris–HCl (containing 0.10 M NaCl, pH 7.4 ± 0.1), at 25 °C. And appropriate baseline corrections in the CD spectra were made.

Attenuated total reflection-Fourier transform infrared (ATR-FTIR) of samples was recorded by FT-IR spectroscopy (AVA TAR 370, Thermo Nicolet Co. of America). The samples were prepared as the followings: 0.5 mL of the liquid from the samples was evaporated on the ZnSe vessel and dried in a vacuum chamber.

The respective blanks of Tris–HCl buffer were used for the correction of all spectra. The above each spectrum was the average of three successive scans.

4. Results and discussion

4.1. Characterization of QDs

The preparation of CdTe/MPA QDs was adopted from literature [31]. The CdTe/MPA QDs precursor was subjected to different refluxing time to control the nanocrystals size. And then, three different CdTe/MPA QDs with maximum emission of 543 nm (green-emitting QDs, GQDs), 579 nm (yellow-emitting QDs, YQDs) and 647 nm (red-emitting QDs, RQDs) were obtained (Fig. 1a). It is worthwhile to note that CdTe/MPA QDs were obtained through ethanol precipitation with centrifugation at 4000 rpm for 5 min; these QDs were treated with ethanol in three repeated cycles to remove the contaminant (unreacted Cd^{2+}, etc.). Besides FL spectra, the absorption spectra are also shown in Fig. 1a. From this figure, we can find that a large red-shift of the maximum absorption and emission peaks took place with the passage of refluxing time. Besides these, the distinctive absorption peak shape was transformed into smooth shoulder peak gradually, and a full width at half-maximum of PL spectra became wider gradually. The above results suggest the diameter of the CdTe/MPA QDs was increasing and the particle size distribution was broadening. The morphology and size of the prepared QDs was studied by TEM (Fig. 1b–d). The shape of these nanoparticles is close to monodisperse, the mean diameter of GQDs, YQDs, and RQDs is about 2.5, 3.5, and 4.5 nm, respectively. Distinct lattice fringes indicating a crystalline product were also observed.

4.2. Effect of QDs on BSA absorption spectra

As we know, the absorption spectra cannot only distinguish between dynamic quenching (collisional process) and static quenching (ground state complex formation), but also get the binding constant (K) of the corresponding reaction [32,33]. So we used the difference absorption spectroscopy to obtain spectra (Fig. 2). The UV–vis absorption spectra of BSA (Fig. 2, curve A) and the difference absorption spectra between BSA/GQDs 1:1 complex and GQDs (Fig. 2, curve D) could not be superposed within experimental error, the results suggest the ground state complex formation. The absorption spectra of BSA in absence and presence of different concentration GQDs, at room temperature (298 K) are shown in Fig. 3a (the data of YQDs and RQDs are not shown). The addition of QDs led to a gradual increase in the absorption intensity of BSA. However, our previous study showed that CdSe QDs led to a minor decrease in the absorption intensity of BSA with the appearance of the isoabsorptive point [7], consistent with other studies [32,34,35]. Since static, but not dynamic quenching (which only affects the excited state of fluorophore) often leads to a change in an absorption spectra via ground state complex formation [33], the above results suggest the ground state complex formation between BSA and QDs. The absorbance change that we observed in the spectrum of the complex was not due to the experimental error because baseline corrections were done for all measurements.

The equilibrium between BSA and QDs is defined by Eqs. (1) and (2),

$$\mathrm{BSA} + \mathrm{QDs} \overset{K_{app}}{\rightleftarrows} \mathrm{BSA} - - - \mathrm{QDs} \tag{1}$$

$$K_{app} = \frac{[\mathrm{BSA} - - - \mathrm{QDs}]}{[\mathrm{BSA}] \cdot [\mathrm{QDs}]} \tag{2}$$

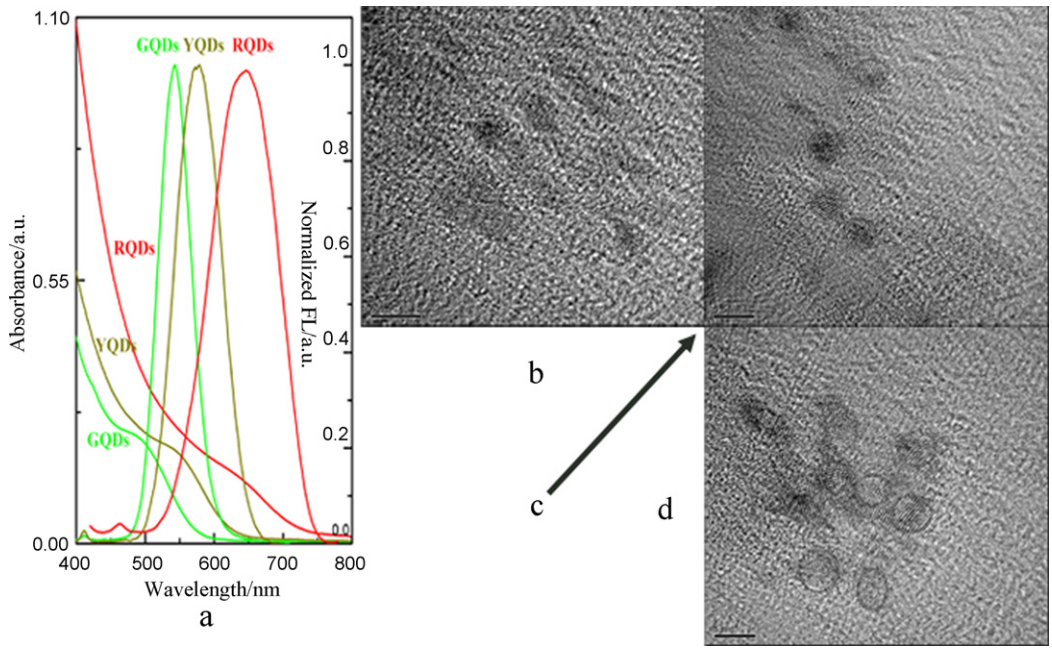

Fig. 1. Absorption and normalized FL spectra of different size (colors: green, yellow, and red) of CdTe/MPA QDs (a) and TEM images of CdTe/MPA QDs with emission of green (b), yellow (c), and red (d) FL.

where K_{app} is the apparent association constant. K_{app} can be obtained from the changes of the intensity of absorption and expressed as Eq. (3) [32,35,36]:

$$\frac{1}{A-A_0} = \frac{1}{A_C-A_0} + \frac{1}{K_{app}} \cdot \frac{1}{A_C-A_0} \cdot \frac{1}{[QDs]} \quad (3)$$

where A, A_0, A_c are the absorbance of BSA containing different concentrations of QDs, BSA and the complex, respectively. The values of $1/(A-A_0)$ were calculated and plotted against quencher concentration 1/[QDs] according to Eq. (3) as shown in Fig. 3b. After a linear fit, the slope equals the value of $1/K_{app}\cdot 1/(A_c-A_0)$ with an intercept of $1/(A_c-A_0)$ on the ordinate. The calculated value of K_{app} is $1.72\times10^5\,M^{-1}$ (GQDs), $1.95\times10^5\,M^{-1}$ (YQDs), and $5.93\times10^5\,M^{-1}$ (RQDs), respectively (correlation coefficient $R>0.9900$). These results suggest that the effect of QDs with different sizes on BSA absorbance was different from each other. The apparent association constant between RQDs and BSA was higher than that of YQDs and GQDs, that is, the larger size is, the stronger binding force is.

4.3. Effect of QDs on BSA FL spectra

FL quenching efficiency and aspects of the quenching mechanism of the BSA by QDs were studied by FL measurements. The quenching FL is known to occur by excited state reactions, energy transfer, collisional quenching (dynamic quenching) and complex formation (static quenching)[33]. Both dynamic quenching and static quenching reveal the connection of linearity between relative FL intensity (F_0/F) and QDs concentration. The quenching of BSA FL by QDs can be described by a Stern–Volmer equation:

$$\frac{F_0}{F} = 1 + K_{sv}[Q] \quad (4)$$

where F_0 and F are the FL intensity of BSA in the absence and presence of QDs respectively, [Q] is the QDs concentration and K_{sv} is the Stern–Volmer quenching constant.

Fig. 4 displays FL spectra of BSA with various concentrations of YQDs/MPA at 298 K (other data of GQDs/MPA and RQDs/MPA are not shown). The observed FL band centered around 350 nm. The FL intensity was significantly quenched by the addition of YQDs/MPA when the concentration of BSA is 10 μM. Because YQDs/MPA's emission wavelengths are much farther away from the BSA absorption and emission wavelengths, the emission of YQDs/MPA between 290 and 450 nm is not considered. Our results suggest that the quenching effect of YQDs/MPA on the FL emission of BSA is the concentration dependent, and YQDs/MPA can bind to the BSA. Furthermore, it was observed that the FL intensity of YQDs/MPA was nearly zero compared with BSA in the wavelength range of 290–450 nm upon excitation at 280 nm (Fig. 4).

The ratios F_0/F were calculated and plotted against quencher concentration according to Eq. (5) at 298 K as shown in Fig. 5a. After a linear fit, K_{sv} (~10^5 L/mol) was calculated from the slope of the plots. The Stern–Volmer quenching constant between RQDs and BSA was higher than that of YQDs and GQDs, which is identical to

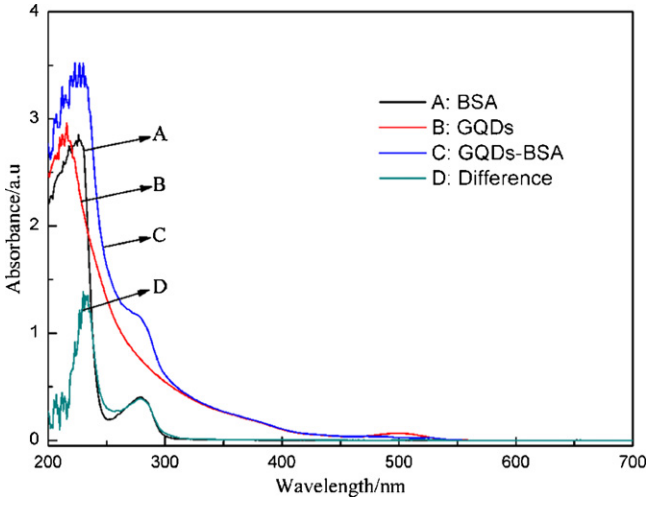

Fig. 2. UV–visible spectra of BSA in the presence of GQDs: A, absorption spectrum of BSA only; B, absorption spectrum of QDs only; C, absorption spectrum of GQDs–BSA 1:1 complex; D, difference between absorption spectrum of GQDs–BSA 1:1 complex and QDs. c(BSA) = c(QDs)) 1.0×10^{-5} M.

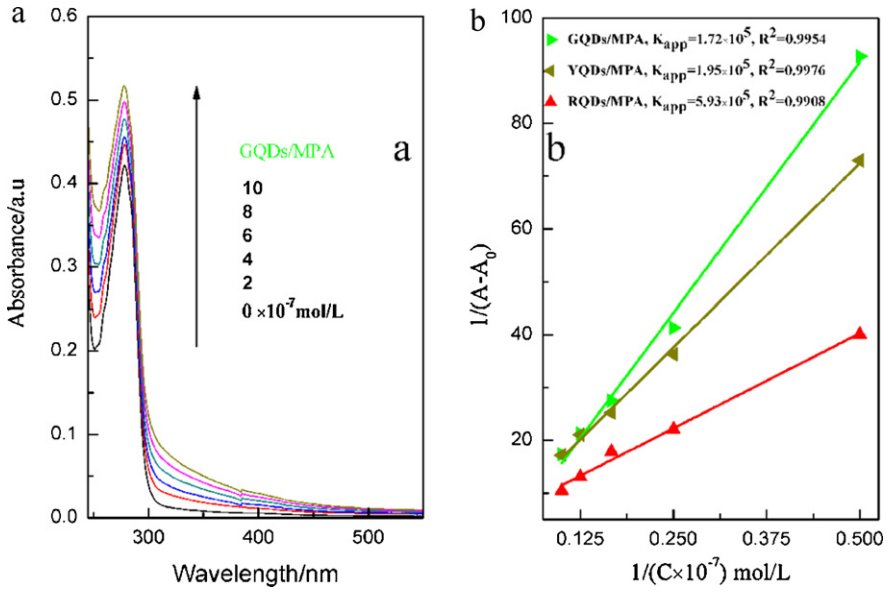

Fig. 3. Absorption spectra of BSA in the presence of GQDs, YQDs, and RQDs in the concentration range of (0–10) × 0.1 μM (a), the straight line dependence of $1/(A - A_0)$ on the reciprocal concentration of different size QDs (b).

the absorption spectral results. The result suggests that QDs can effectively quench the FL of BSA in a size-dependent manner.

Because the fluorescence life time (τ_0) of the bimolecular is 10^{-8} s, the dimolecular quenching constants K_q ($K_{sv} = K_q \cdot \tau_0$) of GQDs, YQDs, and RQDs for BSA were calculated to be 1.72×10^{13}, 1.93×10^{13}, and 3.32×10^{13} L/(mol s), respectively [33]. As we know, the large diffusion and collision constant of various quenchers with the biological macromolecules is 10^{10} L/(mol s) (dynamic quenching). Considering that in our experiment the rate constants of the BSA quenching procedure initiated by QDs were much greater than 10^{10} L/(mol s), it can be concluded that the nature of quenching is not dynamic but probably static, resulting in forming QDs–BSA complexes [37].

4.4. Binding constants and the number of binding sites

The binding constants were calculated according to the double-logarithm equation (Eq. (5)) [32,38],

$$\log\left[\frac{F_0 - F}{F}\right] = \log K + n \log[Q] \tag{5}$$

where K is the binding constant and n is the number of binding sites per BSA. Fig. 5b shows the double-logarithm curves of different sizes QDs quenching BSA fluorescence at 298 K. From this figure, the binding constants and the number of binding sites between RQDs and BSA were higher than those of YQDs and GQDs. The results illustrate that the size of CdTe QDs affected the affinity for BSA and the increasing size of QDs enhanced the binding force with BSA. K was calculated at different temperatures according to Eq. (5) as shown in Table 1. The results show the binding constant K is inversely correlated with temperature. Due to dynamic quenching depends on diffusion, and the coefficient of diffusion will increase with increasing temperature, the binding constant is directly correlated with temperature. However, for static quenching, the stability of complex formation will decrease with increasing temperature, causing the quenching constant to be inversely correlated with the temperature. Thus, our results also suggest that the quenching mechanism is static in nature. The number of binding sites is about 1 for different sizes QDs, in agreement with other authors [22,28], suggesting there is only one type of interaction between BSA and QDs.

4.5. The determination of the force acting between QDs and BSA

In general, the interaction between endogenous or exogenous ligands and biological macromolecules is a complex process that involves not only electrostatic interactions, multiple hydrogen bonds, and van der Waals force, but also hydrophobic, π–π stacking and so forth [22,23,39,40]. Ross and Subramanian [41] thought that electrostatic interactions are important if the enthalpy change (ΔH) is negative; and the entropy change (ΔS) < 0 results from common characteristics of hydrogen bond and van der Waals force. Thus, to study the interaction between QDs and BSA, the thermodynamic parameters were calculated from the van't Hoff plots. If the ΔH is temperature independent in the temperature range studied, both ΔH and ΔS can be calculated from the van't Hoff equation (Eq. (6)); Furthermore, the temperature range cannot change too much, or else the protein will be denatured, and the temperature range we chose is widely used in previous study [22,23,42].

$$\ln K = -\frac{\Delta H}{RT} + \frac{\Delta S}{R} \tag{6}$$

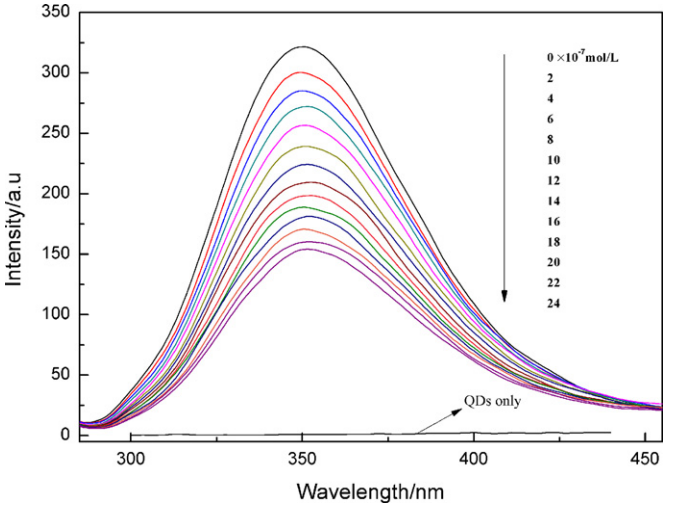

Fig. 4. Fluorescence emission spectra of YQDs/MPA-BSA complex in the presence of different concentrations YQDs/MPA in Tris–HCl buffer solution after exciting it at 280 nm.

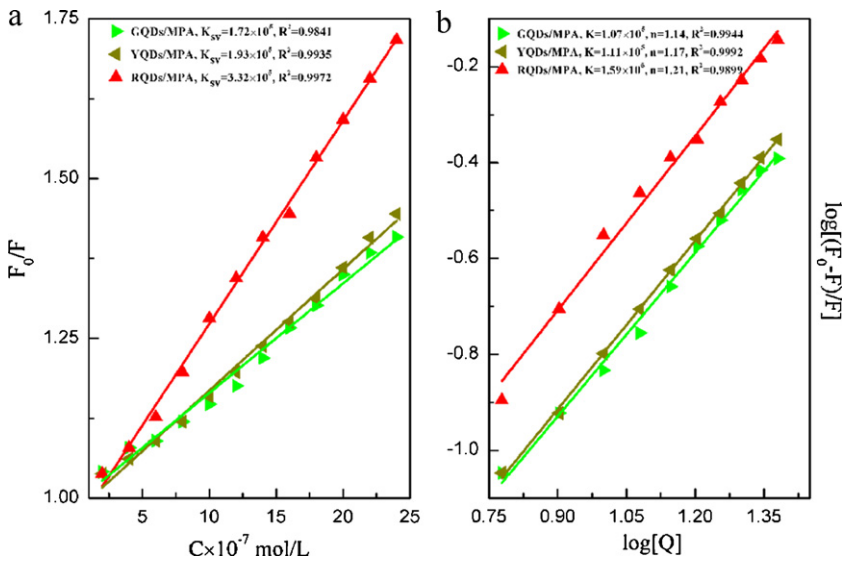

Fig. 5. Stern–Volmer plots (a), binding constant (K), and binding sites (n, b) for the quenching of BSA by different size QDs at 298 K.

where ΔH and ΔS are the standard enthalpy and entropy change for the reaction, respectively, R is the gas constant and T is the temperature. The values of ln K were plotted against $1/T$ according to Eq. (6) at different temperatures as shown in Fig. 6. ΔH and ΔS were calculated at different temperatures according to the slope and the intercept as shown in Table 1. Using the relationship $\Delta G = \Delta H - T\Delta S$, the free energy change (ΔG) was estimated as also shown in Table 1.

As we know, all chemical, physical, and biological processes are accompanied by a change in thermodynamic parameters (ΔG, ΔH, and ΔS) [43,44]. Table 1 shows the values of thermodynamic parameters ($\Delta G < 0$, $\Delta H < 0$, $\Delta S > 0$), the negative values of ΔG suggest that the binding process of QDs to BSA is spontaneous, $\Delta H < 0$ and $\Delta S > 0$ suggest that the intermolecular bond energies is decreasing and the disorder of the system is increasing. So the interaction between QDs and BSA would certainly happen. The results indicate that electrostatic interactions play a major role in the binding reaction between BSA and QDs. It also was proved by Liu's results [23], because the electrostatic interactions occurred between the negatively charged QDs and the cationic "hot spot" around the active site of the protein (human serum albumin, HSA). Furthermore, the hydrophobic interactions are also important [22,45].

4.6. Energy transfer between BSA and QDs

From Figs. 1 and 4, there is an overlap between the FL emission band of BSA and an excitation band of three QDs. So we can calculate the distance between the QDs binding sites and the fluorophore (BSA) according to Förster theory of molecular resonance energy transfer. According to this theory, the efficiency of energy transfer between the donor and acceptor, E, could be calculated by Eq. (7) [46,47].

$$E = 1 - \frac{F}{F_0} = \frac{R_0^6}{R60 + r^6} \tag{7}$$

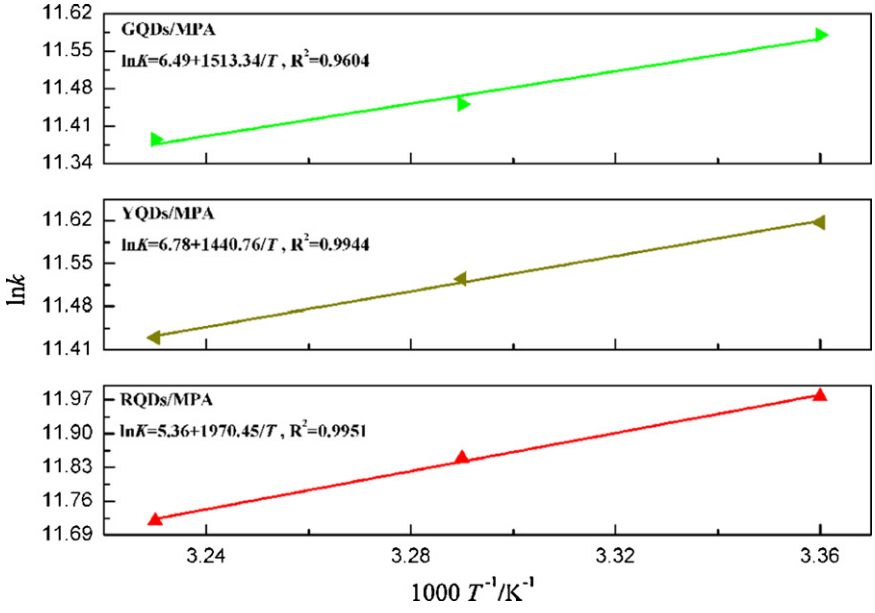

Fig. 6. Van't Hoff plots of QDs–BSA system.

Table 1
The binding constants (K) and thermodynamic parameters of QDs–BSA system at different temperatures.

QDs	GQDs/MPA			YQDs/MPA			RQDs/MPA		
T/K	298	304	310	298	304	310	298	304	310
K ($\times 10^5$ L/mol, R^2)	1.07 (0.9944)	0.94 (0.9889)	0.88 (0.9910)	1.11 (0.9849)	1.03 (0.9875)	0.92 (0.9775)	1.59 (0.9899)	1.40 (0.9875)	1.23 (0.9900)
ΔG kJ/mol	−28.66	−28.98	−29.31	−28.78	−29.12	−29.45	−29.66	−29.93	−30.19
ΔH kJ/mol	−12.58			−11.98			−16.38		
ΔS J/(mol K)	53.96			56.37			44.56		

where r is the distance between the donor and acceptor, and R_0 is the critical distance when the efficiency of transfer is 50%.

$$R_0^6 = 8.8 \times 10^{-25}\,\kappa^2\, n^{-4}\,\phi J \tag{8}$$

In Eq. (8), κ^2 is the orientation factor related to the geometry of the donor and acceptor of dipoles and $\kappa^2 = 2/3$ for random orientation as in fluid solution; n is the average refracted index of medium in the wavelength range where spectral overlap is significant; ϕ is the FL quantum yield of the donor; J is the effect of the spectral overlap between the emission spectrum of the donor and the absorption spectrum of the acceptor, which could be calculated by the equation:

$$J = \frac{\int_0^\infty F(\lambda)\varepsilon(\lambda)\lambda^4 d\lambda}{\int_0^\infty F(\lambda)d\lambda} \tag{9}$$

where $F(\lambda)$ is the corrected FL intensity of the donor in the wavelength range, from λ to $\lambda + \Delta\lambda$; $\varepsilon(\lambda)$ is the extinction coefficient of the acceptor at λ.

In the present case, $n = 1.36$, $\phi = 0.1$ [48], according to Eqs. (7)–(9), R_0 and r could be calculated (GQDs (4.06 and 4.80 nm), YQDs (4.11 and 4.82 nm), and RQDs (4.32 and 4.87 nm)), respectively. The values for R_0 and r are on the 2–8 nm scale, and $0.5R_0 < r < 1.5R_0$, indicating an existence of an interaction between QDs and BSA. It also suggested that the binding of QDs to BSA is through energy transfer [49].

4.7. CD spectra study

In order to verify the binding of CdTe QDs to BSA, the CD technique was applied. As we know, the CD spectra of HSA exhibited two negative bands in the UV region at 208 and 222 nm. The band is characteristic of an α-helical structure of protein. The peak at 220 nm is contributed by the $n \rightarrow \pi^*$ transition of peptide bonds in the α-helix, and the peak at 208 nm is contributed by $\pi \rightarrow \pi^*$ transitions of the peptide bonds on the α-helices[17]. The CD results were expressed in terms of mean residue ellipticity (MRE) in deg cm^2 dmol^{-1} according to Eq. (10):

$$\mathrm{MRE} = \frac{\text{Observed CD}\,(m\,\text{deg})}{C_p n l \times 10} \tag{10}$$

where C_p is the molar concentration of the protein, n the number of amino acid residues (583 for BSA) and l is the path length (0.1 cm). Fig. 7 shows the far-UV CD spectra of BSA after addition of different size QDs. It can be seen that the negative peak decreases gradually

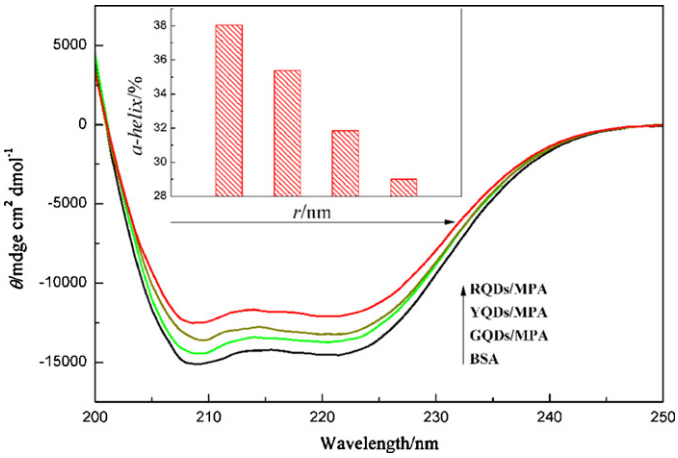

Fig. 7. The far-UV CD spectra of the QDs–BSA system, BSA concentration was 1.0×10^{-5} mol/L, the QDs concentration was 1.0×10^{-6} mol/L. The inset shows the α-helicity of BSA versus the different sizes QDs at 208 nm.

Table 2
Fractions of different secondary structures determined by SELCON3.

QDs	Percentage of secondary structure					
	α-helix		β-strand		Turn	Unordered
	α^R	α^D	β^R	β^D		
BSA	26.5	16.2	8.0	5.9	18.7	26.5
BSA + GQDs	25.8	16.5	6.9	5.5	18.6	26.3
BSA + YQDs	24.1	15.9	7.4	5.8	18.9	27.2
BSA + RQDs	22.6	16.0	7.9	6.3	19.8	28.7

The superscripts "R" and "D" represent "ordered" and "disordered", respectively.

with the size of QDs increasing from 2.29 to 4.07 nm. Therefore, we can deduce that the molecular structure of BSA is changed by QDs. The α-helical contents of free and combined BSA were also calculated from MRE values at 208 nm using Eq. (11) [23]:

$$\alpha\text{-helix}(\%) = \frac{-\text{MRE}_{208} - 4000}{33000 - 4000} \quad (11)$$

where MRE_{208} is the observed MRE value at 208 nm, 4000 is the MRE of the β-form and random coil conformation cross at 208 nm, and 33,000 is the MRE value of a pure α-helix at 208 nm. The inset of Fig. 7 shows the helicity of BSA versus the size of QDs at 208 nm. We can conclude that the helicity of BSA decreased significantly with increasing the size of QDs, which suggests a stronger structural change.

Further, in order to quantify the different types content of secondary structures, far-UV CD spectra have been analyzed by the algorithm SELCON3. Table 2 shows the fractions of different secondary structures after addition of different size QDs. An apparent decreasing tendency of the α-helices content and an increasing tendency of β-strands, turn, and unordered structure contents could be observed (Table 2). As known, the secondary structure contents are related close to the biological activity of the protein, thus a decrease in α-helical implied the loss of the biological activity of BSA upon interaction with the different size of QDs. The conformation changes here implied that the serum albumin would adopt a more incompact conformation state on the surface of QDs and resulted in the exposure of the hydrophobic cavities.

4.8. ATR-FTIR characterization

As we know, ATR-FTIR spectroscopy offers another valuable method to monitor the changes in the secondary structure of proteins when interacted with ligands (QDs). Usually the amide I peak position of BSA occurs in the region of 1600–1700 cm^{-1} (mainly C═O stretch), and its main absorption is due to the stretching vibration of amino acid residue and the hydrogen bond formed by carbonyl and hydrogen in acid amides. The amide II band usually occurs in the region of 1500–1550 cm^{-1} which includes C—N stretch coupled with N—H bending mode, and it is an important band to reflect the structure of proteins [50]. Fig. 8 shows the ATR-FTIR spectrum of BSA in the absence and presence of three QDs. As can be seen from the ATR-FTIR spectrum, the peak position of amide I moved from 1643 to 1654 cm^{-1} and amide II moved from 1523 to 1535 cm^{-1} when BSA was interacted with three QDs. Though the peak position changed a little between GQDs–BSA, YQDs–BSA, and RQDs–BSA, the results suggested that the secondary structure change of the BSA had been induced by QDs [50,51].

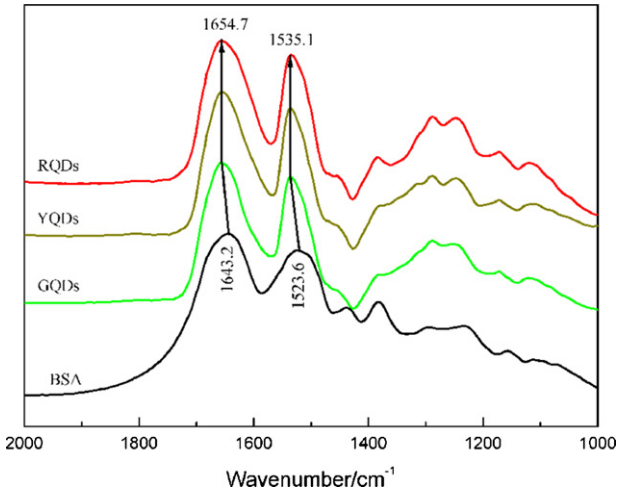

Fig. 8. The ATR-FTIR spectra of BSA in the absence and presence of QDs.

5. Conclusion

The biological effects of three size CdTe QDs to BSA have been investigated mainly by FL spectra, UV–vis absorption spectra and circular dichroism (CD). The Stern-Volmer quenching constant (K_{sv}) at different temperatures, corresponding thermodynamic parameters (ΔH, ΔG and ΔS), and information of the structural features of BSA were gained. We found that QDs can effectively quench the FL of BSA in a size-dependent manner, electrostatic interactions play a major role in the binding reaction, and the nature of quenching is static, resulting in forming QDs–BSA complexes. The CD and ATR-FTIR spectra showed that the secondary structure of BSA was changed by QDs. This study contributes to a better understanding of the size effects on QDs-proteins interactions, which is a critical issue for applications in vivo.

Acknowledgements

We gratefully acknowledge the financial support of supported by the Fundamental Research Funds for the Central Universities (2011-Ia-035), National Natural Science Foundation of China (No. 51175394), Ministry of Education of China (PCSIRT0644), and China Scholarship Council.

References

[1] L.E. Brus, A simple model for the ionization potential electron affinity and aqueous redox potentials of small semiconductor crystallites, J. Chem. Phys. 79 (1983) 5566–5571.
[2] S. Coe, W.K. Woo, M. Bawendi, V. Bulovic, Electroluminescence from single monolayers of nanocrystals in molecular organic devices, Nature 420 (2002) 800–803.
[3] M.A. El-Sayed, Small is different: shape-, size-, and composition-dependent properties of some colloidal semiconductor nanocrystals, Acc. Chem. Res. 37 (2004) 326–333.
[4] M. Bruchez Jr., M. Moronne, P. Gin, S. Weiss, A.P. Alivisatos, Semiconductor nanocrystals as fluorescent biological labels, Science 281 (1998) 2013–2015.
[5] W.C.W. Chan, S. Nie, Quantum dot bioconjugates for ultrasensitive nonisotopic detection, Science 281 (1998) 2016–2018.
[6] X. Michalet, F.F. Pinaud, L.A. Bentolila, J.M. Tsay, S. Doose, J.J. Li, G. Sundaresan, A.M. Wu, S.S. Gambhir, S. Weiss, Quantum dots for live cells, in vivo imaging, and diagnostics, Science 307 (2005) 538–544.
[7] P. Liu, Q.S. Wang, X. Li, Studies on CdSe/L-cysteine quantum dots synthesized in aqueous solution for biological labeling, J. Phys. Chem. C 113 (2009) 7670–7676.
[8] R. Kikkeri, B. Lepenies, A. Adibekian, P. Laurino, P.H. Seeberger, In vitro imaging and in vivo liver targeting with carbohydrate capped quantum dots, J. Am. Chem. Soc. 131 (2009) 2110–2112.
[9] T. Fu, H.-Y. Qin, H.-J. Hu, Z. Hong, S. He, Aqueous synthesis and fluorescence-imaging application of CdTe/ZnSe core/shell quantum dots with high stability and low cytotoxicity, J. Nanosci. Nanotechnol. 10 (2010) 1741–1746.
[10] J. Lovric, S.J. Cho, F.M. Winnik, D. Maysinger, Unmodified cadmium telluride quantum dots induce reactive oxygen species formation leading to multiple organelle damage and cell death, Chem. Biol. 12 (2005) 1227–1234.
[11] C. Kirchner, T. Liedl, S. Kudera, T. Pellegrino, A.M. Javier, H.E. Gaub, S.S. llzle, N. Fertig, W.J. Parak, Cytotoxicity of colloidal CdSe and CdSe/ZnS nanoparticles, Nano Lett. 5 (2005) 331–338.

[12] S.J. Cho, D. Maysinger, M. Jain, B. Roder, S. Hackbarth, F.M. Winnik, Long-term exposure to CdTe quantum dots causes functional im-pairments in live cells, Langmuir 23 (2007) 1974–1980.
[13] Y. Su, M. Hu, C. Fan, Y. He, Q. Li, W. Li, L. Wang, P. Shen, Q. Huang, The cytotoxicity of CdTe quantum dots and the relative contributions from released cadmium ions and nanoparticle properties, Biomaterials 31 (2010) 4829–4834.
[14] S.J. Tan, N.R. Jana, S. Gao, P.K. Patra, J.Y. Ying, Surface-ligand-dependent cellular interaction subcellular localization, and cytotoxicity of polymer-coated quantum dots, Chem. Mater. 22 (2010) 2239–2247.
[15] C. Wang, X. Gao, X. Su, Study the damage of DNA molecules induced by three kinds of aqueous nanoparticles, Talanta 80 (2010).
[16] Zhang, W. Yao, Y. Chen, Y. Imaging, Quantifying the morphology and nanoelectrical properties of quantum dot nanoparticles interacting with DNA, J. Phys. Chem. C 115 (2011) 599–606.
[17] L. Zhao, R. Liu, X. Zhao, B. Yang, C. Gao, X. Hao, Y. Wu, New strategy for the evaluation of CdTe quantum dot toxicity targeted to bovine serum albumin, Sci. Total Environ. 407 (2009) 5019–5023.
[18] M.M. Dzagli, V. Canpean, M. Iosin, M.A. Mohou, S. Astilean, Study of the interaction between CdSe/ZnS core-shell quantum dots and bovine serum albumin by spectroscopic techniques, J. Photochem. Photobiol. A 215 (2010) 118–122.
[19] L. Shao, C. Dong, F. Sang, H. Qian, J. Ren, Studies on interaction of CdTe quantum dots with bovine serum albumin using fluorescence correlation spectroscopy, J Fluoresc. 19 (2009) 151–157.
[20] M. Ghali, Static quenching of bovine serum albumin conjugated with small size CdS nanocrystalline quantum dots, J. Lumin. 130 (2010) 1254–1257.
[21] X.-C. Shen, X.-Y. Liou, L.-P. Ye, H. Liang, Z.-Y. Wang, Spectroscopic studies on the interaction between human hemoglobin and CdS quantum dots, J. Colloid Interface Sci. 311 (2007) 400–406.
[22] L. Ding, P.J. Zhou, S.Q. Li, G.Y. Shi, T. Zhong, M. Wu, Spectroscopic studies on the thermodynamics of L-cysteine capped CdSe/CdS quantum dots – BSA interactions, J Fluoresc. 21 (2011) 17–24.
[23] Q. Xiao, S. Huang, Z.D. Qi, B. Zhou, Z.K. He, Y. Liu, Conformation, thermodynamics and stoichiometry of HSA adsorbed to colloidal CdSe/ZnS quantum dots, Biochim. Biophys. Acta, Proteins Proteomics. 1487 (2008) 1020–1027.
[24] J.-G. Liang, X.-P. Ai, Z.-K. He, D.-W. Pang, Functionalized CdSe quantum dots as selective silver ion chemodosimeter, Analyst 129 (2004) 619–622.
[25] N.N. Mamedova, N.A. Kotov, Albumin-CdTe nanoparticle bioconjugates: preparation, structure, and interunit energy transfer with antenna effect, Nano Lett. 1 (2001) 281–286.
[26] X. Huang, L. Li, H. Qian, C. Dong, J. Ren, A resonance energy transfer between chemiluminescent donors and luminescent quantum-dots as acceptors, Angew. Chem. Int. Ed. 45 (2006) 5140–5143.
[27] J. Liang, Y. Cheng, H. Han, Study on the interaction between bovine serum albumin and CdTe quantum dots with spectroscopic techniques, J. Mol. Struct. 892 (2008) 116–120.
[28] Xiao, J. Bai, Y. YuanfengWang, Chen, J. XinlinWei, Systematic investigation of the influence of CdTe QDs size on the toxic interaction with human serum albumin by fluorescence quenching method, Spectrochim. Acta A 76 (2010) 93–97.
[29] J. Xiao, T. Chen, L. Chen, H. Cao, F. Yang, Y. Bai, CdTe quantum dots (QDs) improve the affinities of baicalein and genistein for human serum albumin *in vitro*, J. Inorg. Biochem. 104 (2010) 1148–1155.
[30] Q. Wang, F. Ye, T. Fang, W. Niu, P. Liu, X. Min, X. Li, Bovine serum albumin-directed synthesis of biocompatible CdSe quantum dots and bacteria labeling, J. Colloid Interface Sci. 355 (2011) 9–14.
[31] L. Li, H. Qian, N. Fang, J. Ren, Significant enhancement of the quantum yield of CdTe nanocrystals synthesized in aqueous phase by controlling the pH and concentrations of precursor solutions, J. Lumin. 116 (2006) 59–66.
[32] M.A. Jhonsi, A. Kathiravan, R. Renganathan, Spectroscopic studies on the interaction of colloidal capped CdS nanoparticles with bovine serum albumin, Colloids Surf. B 72 (2009) 167–172.
[33] J.R. Lakowicz, Principles of Fluorescence Spectroscopy, 3rd ed., Springer, New York, 2006.
[34] M. Idowu, E. Lamprecht, T. Nyokong, Interaction of water-soluble thiol capped CdTe quantum dots and bovine serum albumin, J. Photochem. Photobiol. A 198 (2008) 7–12.
[35] A. Kathiravan, R. Renganathan, Interaction of colloidal TiO_2 with bovine serum albumin: a fluorescence quenching study, Colloids Surf. A 324 (2008) 176–180.
[36] H.A. Benesi, J.H. Hildebrand, A spectrophotometric investigation of the interaction of iodine with aromatic hydrocarbons, J. Am. Chem. Soc. 71 (1949) 2703–2707.
[37] J.G. Xu, Z.B. Wang, Fluorimetry, 3rd ed., Science Press, Beijing, 2006.
[38] V. Anbazhagan, R. Renganathan, Study on the binding of 2,3-diazabicyclo[2.2.2]oct-2-ene with bovine serum albumin by fluorescence spectroscopy, J. Lumin. 128 (2008) 1454–1458.
[39] M. De, C.C. You, S. Srivastava, V.M. Rotello, Biomimetic interactions of iroteins with functionalized nanoparticles: a thermodynamic study, J. Am. Chem. Soc. 129 (2007) 10747–10753.
[40] D. Leckband, Measuring the forces that control protein interactions, Annu. Rev. Biophys. Biomol. Struct. 29 (2000) 1–26.
[41] D.P. Ross, S. Subramanian, Thermodynamics of protein association reactions: forces contributing to stability, Biochemistry 20 (1981) 3096–3102.
[42] R. Mahtab, H.H. Harden, C.J. Murphy, Temperature- and salt-dependent binding of long DNA to protein-sized quantum dots: thermodynamics of inorganic protein–DNA interactions, J. Am. Chem. Soc. 122 (2000) 14–17.
[43] P. Liu, Q.S. Wang, X. Li, C.C. Zhang, Zeta-potentials and enthalpy changes in the process of electrostatic self-assembly of cations on silica surface, Powder Technol. 193 (2009) 46–49.
[44] A.R. Cestaria, E.F.S. Vieiraa, J.A. Simonib, C. Airoldi, Thermochemical investigation on the adsorption of some divalent cations on modified silicas obtained from sol–gel process, Thermochim. Acta 348 (2000) 25–31.
[45] X. Jiang, J. Jiang, Y. Jin, E. Wang, S. Dong, Effect of colloidal gold size on the conformational changes of adsorbed cytochrome c: probing by circular dichroism, UV–visible, and infrared spectroscopy, Biomacromolecules 6 (2005) 46–53.
[46] L.A. Sklar, B.S. Hudson, R.D. Simoni, Conjugated polyene fatty acids as fluorescent probes: synthetic phospholipid membrane studies, Biochemistry 16 (1977) 819–828.
[47] L. Stryer, Fluorescence energy transfers as a spectroscopic ruler, Annu. Rev. Biochem. 47 (1978) 819–846.
[48] G. Qing-Lian, L. Ran, J. Feng-Lei, T. Jian-Cheng, L. Lin-Wei, L. Yi, Characterization of the interactions between itraconazole and human and bovine serum albumins by a spectroscopic method, Acta Phys. Chim. Sin. 25 (2009) 2147–2154.
[49] Q. Xiao, S. Huang, Z.D. Qi, B. Zhou, Z.K. He, Y. Liu, Conformation, thermodynamics and stoichiometry of HSA adsorbed to colloidal CdSe/ZnS quantum dots, Biochim. Biophys. Acta 1784 (2009) 1020–1027.
[50] P. Ju, H. Fan, T. Liu, L. Cui, S. Ai, Probing the interaction of flower-like CdSe nanostructure particles targeted to bovine serum albumin using spectroscopic techniques, J. Lumin. 131 (2011) 1724–1730.
[51] B. Zhou, Z.-D. Qi, Q. Xiao, J.-X. Dong, Y.-Z. Zhang, Y. Liu, Interaction of loratadine with serum albumins studied by fluorescence quenching method, J. Biochem. Biophys. Methods 70 (2007) 743–747.